Demonstration of a Mercury Trapped Ion Clock Prototype

Thai M. Hoang, Sang K. Chung, Thanh Le, John D. Prestage, Lin Yi, Robert L. Tjoelker, and Nan Yu
Jet Propulsion Laboratory
California Institute of Technology
Pasadena, CA 91109, USA
Email: Nan.Yu@jpl.nasa.gov

Sehyun Park, Sung-Jin Park, J. Gary Eden
Department of Electrical and Computer Engineering
University of Illinois Urbana-Champaign, IL 61801, USA

Christopher Holland
Applied Sciences Division
SRI International
Menlo Park, CA 94025, USA

***Abstract*—In this work, we report a prototype of micro mercury trapped ion atomic clock. All the clock components have been packaged and demonstrated in a magnetic shield box of 4 liters. The prototype clock shows promising performance with a short-term fractional frequency instability below $\mathbf{10^{-11}\tau^{-1/2}}$ and can reach the $\mathbf{10^{-14}}$-instability level after a day of averaging. The prototype clock is capable of reaching the $\mathbf{10^{-15}}$-fractional frequency instability range. Our demonstration of the integrated clock prototype paves the way for further SWaP reduction and maturation.**

Keywords—atomic frequency standard; mercury ion;

I. INTRODUCTION

There are a number of different approaches for miniaturizing atomic clocks, from vapor-cell-based to trapped atom and ion systems [1]–[12]. Our approach is based on the mercury trapped ion clock, which offers many advantages for miniaturization and performance [13]–[20]. The 40.5-GHz hyperfine transition of the $^{199}Hg^{+}$ ion is one of the highest microwave clock transitions, which provides a high-quality factor for the short-term performance (Fig. 1(a)). The mercury ions can be optically pumped by 194-nm mercury discharge lamps and buffer gas cooled with a few micro-torr of helium. Non-evaporative getter pumps can maintain the vacuum condition required for the trapped ions without the need for an active ion pump. These advantages of mercury-ion clocks are key for the success of the mercury-ion Deep Space Atomic Clock at NASA Jet Propulsion Laboratory, which was launched into low Earth orbit in 2019 [13]–[15].

Previously we demonstrated a 100-cc physics package of a micro mercury trapped ion clock (M2TIC), which includes several key innovations of the M2TIC such as a field-emitter-array (FEA) and ultra-violet (UV) microplasma lamp to reduce the size and power consumption for a mercury trapped ion clock (this work will be published elsewhere). In this paper, we report our latest progress in developing M2TICs. In particular, we have integrated all the components of a M2TIC into a prototype clock package and successfully demonstrated the clock operation. In the following, we will describe our technical approach, clock package, and experimental results.

II. CLOCK PROTOTYPE DESCRIPTION

Mercury trapped ion clocks have been described extensively in the literature [13]–[20]. Here we will briefly describe its working principle. Fig. 1(b) illustrates the basic concept of our microwave mercury trapped ion clock. The atomic reference is the $^{199}Hg^{+}$ ions which are trapped by the linear ion trap. Mercury ions are generated via electron bombardment produced by a field-emitter-array (FEA). The linear trap is housed inside a 15-cc trap tube and driven by a radio frequency (RF) driver. A 450-V peak-to-peak voltage at 1.9 MHz is generally applied to all four trap rods, where the voltages on adjacent trap rods have opposite phases. A potential difference of 17 V is applied between trap rods and the end caps. The construction of the vacuum tube follows the general approach for the DSAC and micro Yb trap tubes [11], [13]. The 40.5-GHz transition between the hyperfine states, $|^2S_{1/2}, F=0\rangle$ and $|^2S_{1/2}, F=1\rangle$, of the trapped ions is used as the clock frequency. A pair of magnetic coils are placed around the trap tube to generate a bias field of about 200 mG (C-field) along the longitudinal direction of the ion trap. A small magnetic shielding encloses the entire vacuum package and coil assembly with openings for optical and electrical accesses.

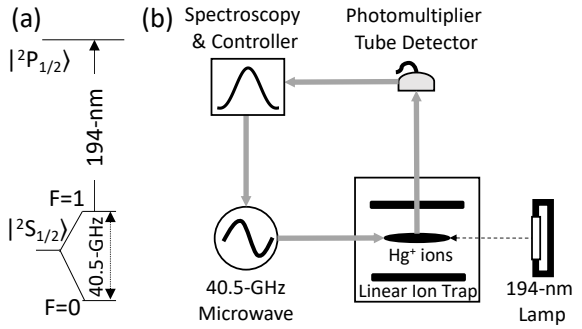

Fig. 1. (a) Simplified energy level of the $^{199}Hg^{+}$ ion. The $|S_{1/2}, F=0\rangle$ and $|S_{1/2}, F=1\rangle$ hyperfine ground states are the upper and lower clock states. (b) Mercury-ion clock concept. $^{199}Hg^{+}$ ions are trapped by a linear RF trap inside a vacuum tube. 40.5-GHz microwave radiation is used to excite the ions from the lower clock state to the upper clock

978-1-6654-3935-0/21/$31.00 ©2021 IEEE

state. A 194-nm light from the $^{202}Hg^+$ lamp optically pumps ions from the upper clock state to the lower clock state through the $|P_{1/2}\rangle$ state. A photomultiplier tube detects the fluorescence photons from the $|P_{1/2}\rangle$ as the upper clock state population. The servo controller locks the microwave frequency to the $^{199}Hg^+$ clock transition.

Other parts of the clock include the 194-nm mercury lamp, microwave source, detection system, microcontroller, and electronic components (Fig. 2(a)). The microwave source is used for probing the 40.5-GHz clock transition. The microwave source consists of a 20.25-GHz frequency synthesizer with a 10-MHz reference from a quartz oscillator. The 20.25-GHz frequency is then doubled and delivered to trapped ions by a microwave waveguide. A micro-plasma mercury lamp is used to optically pump the mercury ions into the lower hyperfine state and for detection purpose. The mercury lamps require a relatively pure ^{202}Hg isotope where the emission of $^{202}Hg^+$ happens to overlap with the transition between the upper hyperfine state to the $|P_{1/2}\rangle$ state of the $^{199}Hg^+$ ion. Light emitted from the lamp is projected onto the trapped ions from one side of the linear trap through a pair of 6-mm diameter, 14-mm focal length lenses. A similar optical arrangement is used to collect the ion fluorescence and direct it onto a solar-blind photomultiplier tube (PMT) detector. The PMT signal is processed by the microcontroller to lock the quartz oscillator to the clock transition of the trapped $^{199}Hg^+$ ions. All the clock components are mounted inside a 4-L mu-metal box (13 cm × 16 cm × 19 cm), which also acts as a second layer of magnetic shield as shown in Fig. 2(b). All the clock components only occupy a fraction of the 4-L box. The small microcontroller would be placed near the PMT detector, but we kept it outside for easy access during this development period. The clock package was powered by external power supplies.

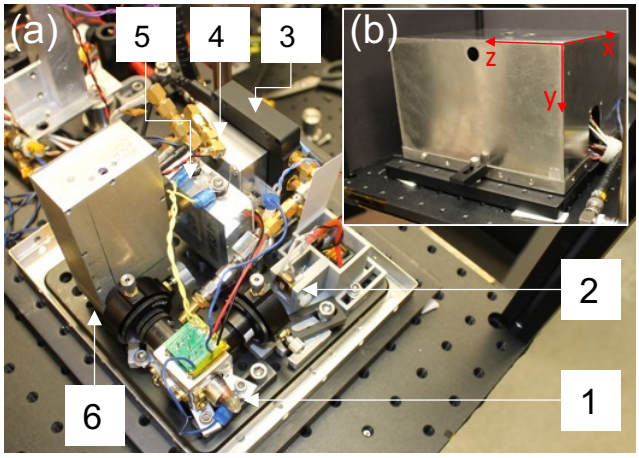

Fig. 2. A photograph of the prototype mercury-ion clock. (a) The clock includes components such as the vacuum package (1), micro-plasma lamp (2), microwave synthesizer (3), Bias-field driver (4), trap RF driver (5), and photomultiplier tube detector (6). (b) The clock components are covered inside a 4-L mu-metal magnetic shield box. Red arrows represent the x-, y-, and z-axis of the clock.

III. RESULTS AND DISCUSSIONS

As the clock components are packed and operated in close proximity, there may be RF interferences between them. In particular, the lamp and trap RF drivers can cause unwanted RF interference onto other components, especially the PMT module. In our case, cover the PMT module with a metal case can provide sufficient protection against RF interference. Nevertheless, it is essential first to verify that the clock prototype can operate properly and meet the short-term and long-term stability requirements of $10^{-11}\tau^{-1/2}$ and a few 10^{-14}, respectively.

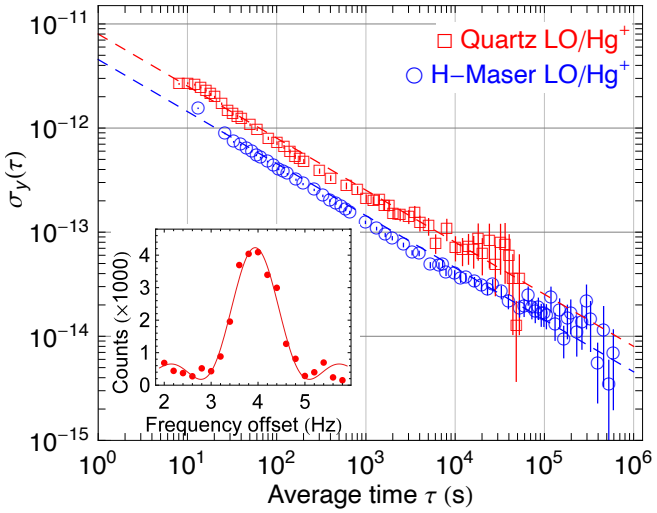

Fig. 3. Allan deviation measurements the prototype clock using a hydrogen maser LO (blue circles) and quartz LO (red squares). Data are fitted to the $\tau^{-1/2}$-function (dashed lines). The errorbars represent the estimated uncertainty of the Allan deviation, which is calculated as $\sigma_y(\tau)/\sqrt{n}$. Here n is the number of measurements. The inset plot shows a typical microwave spectrum with a signal-to-noise ratio of about 9.

To characterize the stability performance, the clock was typically operated in the Rabi mode. In general, microwave clock interrogation time is about 1 s, and the optical pumping/fluorescence collection time is on the order of 4 s. A typical microwave spectrum with an SNR of 9 is shown in the inset of Fig. 3. The FEA can be turned on briefly for about 0.3 s to compensate for the ion loss between each interrogation cycle. A 10-MHz quartz oscillator (Microsemi OX-304) used as the frequency reference for the 40.5-GHz microwave source is locked to the clock transition of the trapped ions. We used a microcontroller to steer the quartz local oscillator (LO) based on the ion signal. Fig. 3 shows that the prototype clock can reach a fractional frequency stability of 4×10^{-14} after averaging for a day with the Allan deviation of $8 \times 10^{-12}\tau^{-1/2}$ (red squares). As the ion lifetime of the clock is over 200 days, in theory, the prototype clock can remain at the 10^{-14}-stability level without reloading ions for days. We also characterized the intrinsic frequency stability of the trapped ions using a hydrogen maser LO. Here we used a 2-second microwave pulse to boost the short-term instability performance and allow the fractional frequency instability to reach the noise floor faster. The fractional frequency instability of trapped ions can reach

the noise floor below the 10^{-14}-level. In particular, the Allan deviation is capable of reaching 6×10^{-15} after averaging for a few days.

Besides the frequency stability, we also demonstrated the robustness in operation of the prototype clock Fig. 4(a) shows that after 20 minutes of loading ions, the frequency of a local oscillator can be locked to the clock transition of the trapped ions. The fractional frequency of the local oscillator moved closer to the clock transition (zero-level) after about 30 minutes. We used a hydrogen maser as the local oscillator to evaluate the intrinsic warm-up time of the mercury-ion system. Here we turned off the power for the clock before the measurement. From the manufacture's specification, the warm-up time of the quartz oscillator is about 5 minutes. The prototype clock should be ready to operate after 20 minutes with the quartz oscillator. We repeated the measurement in Fig. 4(a) several times to evaluate the retrace instability of the prototype clock for about 9 days. The frequency stabilities of the clock were measured after the clock was off for periods varying from 10 to 30 hours. Fig. 4(b) shows the clock transition fractional frequencies of four separate measurements against a hydrogen maser. Comparing the difference between the maximum and minimum fractional frequencies yields a retrace of about 5×10^{-13}.

To lock the local oscillator, the output frequency of the microwave system should be tuned within a lockable range of the clock linewidth. As the prototype clock generally operates with a 1-Hz linewidth, the microwave frequency should be within 1.5 Hz from the 40.5-GHz clock transition. One needs to tune the 10-MHz local oscillator within 0.4 mHz from the absolute 10-MHz frequency. While manually tuning the local oscillator is doable, autonomous tuning will be a useful feature [15]. Fig. 4(c) shows that the prototype clock can autonomously tune the quartz oscillator to bring the 40.5-GHz frequency from 75 Hz away to within the 1-Hz clock linewidth. During the autonomous locking process, the clock linewidth was first broadened with high microwave power to 180 Hz. As a result, the prototype clock can autonomously operate even if the fractional frequency of the quartz oscillator drifts up to 4×10^{-9}. The microwave power was then reduced for a 10-20 Hz linewidth and finally for a 1-Hz linewidth. With the available microwave power, the clock linewidth can be broadened up to 450 Hz to increase the lockable range.

Lastly, we characterize the magnetic sensitivity of the prototype clock. An external magnetic field of about 1 G generated by a magnetic coil is applied to the trapped ion along different directions separately (Fig. 2(a)). As the ions are covered inside the magnetic shield box, and the clock components are packed tightly together, we cannot directly measure the applied field at the ion position with a magnetometer. Instead, we measure the magnetic field generated by the magnetic coil at the oppositive position relative to the trapped ions. To reverse the magnetic field direction, we reverse the current of the magnetic coil. Fig. 4(d) shows that along the x- and z-direction, the magnetic shifts are about 2×10^{-13}/G. Without the magnetic shield, the frequency shift from the second-order Zeeman effect would be about 2×10^{-9}. Here the second-order Zeeman constant is $97 \frac{Hz}{G^2}$. The magnetic shield factor of the prototype clock is about 100. Along the $y$direction, the magnetic shift significantly higher, about 6×10^{-12}/G, since the bias field of the clock is along the y-direction. With a shielding factor of 100, the external field will be reduced to 10 mG inside the trap tube. Adding this 10-mG field on top of the 200-mG bias field, the frequency shift should be 10×10^{-12}, which is consistent with the observation. Since the prototype clock currently has two layers of the magnetic shield, adding two more layers would improve the shielding factor to 10,000. This shielding factor will enable the prototype clock to maintain a 10^{-14}-frequency stability floor even when the external field varies up to 100 mG.

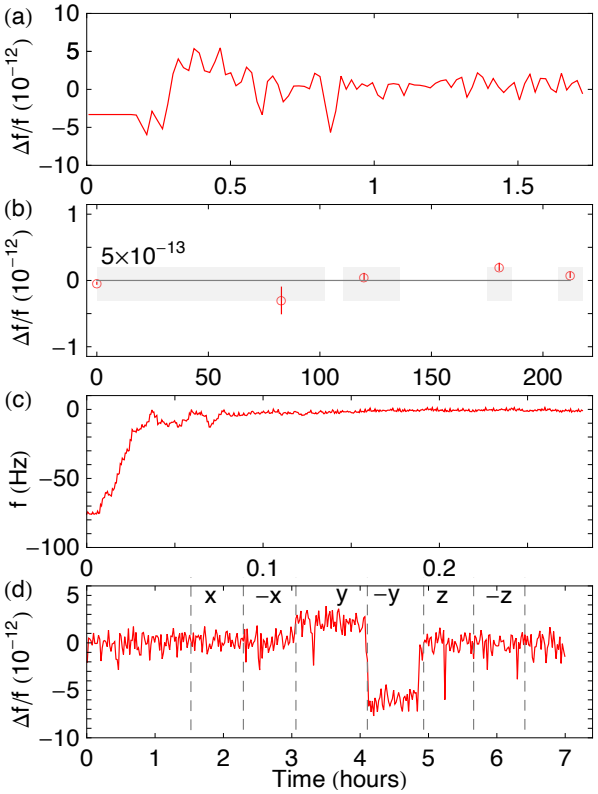

Fig. 4. (a) Warm-up time measurement. After the clock is turned on for about 20 minutes, the frequency of a local oscillator can be locked to the atomic transition of the trapped ions. (b) Retrace measurement. Data points and errorbars represent the mean and corresponding Allan deviation of the fractional frequency for a particular measurement period. The shaded gray regions and their gaps represent the on and off periods of the prototype clock, respectively. The heights of the gray region indicate a retrace instability of 5×10^{-13}. (c) Autolocking demonstration. The prototype clock autonomously tunes the quartz oscillator from 75 Hz away relative to the clock transition to within the locking range of a 1-Hz clock linewidth. (d) External magnetic fields of about 1 G are applied to the trapped ions along different directions. The fractional frequency shifts are about 2×10^{-13}/G along the x- and z-direction and about 6×10^{-12}/G along the y-direction (bias field direction).

IV. CONCLUSIONS

In summary, the prototype clock has demonstrated an Allan deviation of below $10^{-11}\ \tau^{-1/2}$ and the fractional frequency

instability can reach the 10^{-15}-noise floor. The prototype clock showed a retrace of 5×10^{-13} and the warm-up time of 20 minutes. We also demonstrated an autonomous operation where the prototype clock can tune the quartz oscillator from 75 Hz away to within the locking range of a 1-Hz clock linewidth. The successful integration of the clock prototype is an important step toward further size reduction and technology maturation in real-world applications.

ACKNOWLEDGMENT

We are grateful for the support from Blake Tucker for his contributions to the analog electronic development before his retirement from the Jet Propulsion Laboratory. We would like to thank Jacob Gorelik for participating in the development of the microcontroller. We would like to thank William Diener for providing support from the frequency standards test laboratory. The research was carried out at the Jet Propulsion Laboratory, California Institute of Technology, under a contract with the National Aeronautics and Space Administration. Support from the Defense Advanced Research Projects Agency is acknowledged. The views, opinions and/or findings expressed are those of the author and should not be interpreted as representing the official views or policies of the Department of Defense or the U.S. Government. © 2021. California Institute of Technology. Government sponsorship acknowledged.

REFERENCES

[1] J. Sebby-Strabley *et al.*, "Design innovations towards miniaturized GPS-quality clocks," in *2016 IEEE International Frequency Control Symposium, IFCS 2016 - Proceedings*, 2016, doi: 10.1109/FCS.2016.7546775.

[2] X. Liu, E. Ivanov, V. I. Yudin, J. Kitching, and E. A. Donley, "Low-Drift Coherent Population Trapping Clock Based on Laser-Cooled Atoms and High-Coherence Excitation Fields," *Phys. Rev. Appl.*, 2017, doi: 10.1103/PhysRevApplied.8.054001.

[3] P. D. D. Schwindt *et al.*, "Miniature trapped-ion frequency standard with 171Yb+," in *2015 Joint Conference of the IEEE International Frequency Control Symposium and the European Frequency and Time Forum, FCS 2015 - Proceedings*, 2015, doi: 10.1109/FCS.2015.7138951.

[4] B. L. Schmittberger and D. R. Scherer, "A Review of Contemporary Atomic Frequency Standards."

[5] D. R. Scherer *et al.*, "Progress on a miniature cold-atom frequency standard," in *Proceedings of the Annual Precise Time and Time Interval Systems and Applications Meeting, PTTI*, 2014.

[6] S. Knappe *et al.*, "A microfabricated atomic clock," *Appl. Phys. Lett.*, 2004, doi: 10.1063/1.1787942.

[7] R. Lutwak *et al.*, "The Miniature Atomic Clock - Pre-production results," in *Proceedings of the IEEE International Frequency Control Symposium and Exposition*, 2007, doi: 10.1109/FREQ.2007.4319292.

[8] L. Maleki *et al.*, "All-Optical Integrated rubidium Atomic Clock," in *Proceedings of the IEEE International Frequency Control Symposium and Exposition*, 2011, doi: 10.1109/FCS.2011.5977304.

[9] G. Phelps, N. Lemke, C. Erickson, J. Burke, and K. Martin, "Compact Optical Clock with 5×10−13 Instability at 1 s," *Navig. J. Inst. Navig.*, 2018, doi: 10.1002/navi.215.

[10] Z. Newman *et al.*, "Photonic integration of an optical atomic clock," *Optica*, 2018, doi: 10.1364/OPTICA.6.000680.

[11] Y. Y. Jau, H. Partner, P. D. D. Schwindt, J. D. Prestage, J. R. Kellogg, and N. Yu, "Low-power, miniature 171Yb ion clock using an ultra-small vacuum package," *Appl. Phys. Lett.*, 2012, doi: 10.1063/1.4767454.

[12] P. D. D. Schwindt *et al.*, "A highly miniaturized vacuum package for a trapped ion atomic clock," *Rev. Sci. Instrum.*, 2016, doi: 10.1063/1.4948739.

[13] J. D. Prestage, M. Tu, S. K. Chung, and P. MacNeal, "Compact microwave mercury ion clock for space applications," in *2008 IEEE International Frequency Control Symposium, FCS*, 2008, doi: 10.1109/FREQ.2008.4623080.

[14] J. D. Prestage, S. K. Chung, R. J. Thompson, and P. MacNeal, "Progress on small mercury ion clock for space applications," in *2009 IEEE International Frequency Control Symposium Joint with the 22nd European Frequency and Time Forum*, 2009, doi: 10.1109/FREQ.2009.5168141.

[15] R. L. Tjoelker *et al.*, "Mercury ion clock for a NASA technology demonstration mission," *IEEE Trans. Ultrason. Ferroelectr. Freq. Control*, 2016, doi: 10.1109/TUFFC.2016.2543738.

[16] T. Bandi, J. Prestage, S. Chung, T. Le, and N. Yu, "Demonstration of Long Vacuum Integrity Lifetime of a Trapped Ion Clock Package," *Interplanet. Netw. Prog. Rep.*, vol. 204, pp. 1–9, 2016.

[17] T. A. Ely, E. A. Burt, J. D. Prestage, J. M. Seubert, and R. L. Tjoelker, "Using the Deep Space Atomic Clock for Navigation and Science," *IEEE Trans. Ultrason. Ferroelectr. Freq. Control*, 2018, doi: 10.1109/TUFFC.2018.2808269.

[18] G. Kaur Gulati *et al.*, "Miniatured and Low Power Mercury Microwave Ion Clock," in *IFCS 2018 - IEEE International Frequency Control Symposium*, 2018, doi: 10.1109/FCS.2018.8597538.

[19] T. M. Hoang *et al.*, "Performance of Micro Mercury Trapped Ion Clock," in *2019 Joint Conference of the IEEE International Frequency Control Symposium and European Frequency and Time Forum (EFTF/IFC)*, 2019, pp. 1–2, doi: 10.1109/FCS.2019.8856065.

[20] T. M. Hoang *et al.*, "Stability Demonstration of a 15-cc Mercury-Ion Vacuum Trap Tube," in *IFCS-ISAF 2020 - Joint Conference of the IEEE International Frequency Control Symposium and IEEE International Symposium on Applications of Ferroelectrics, Proceedings*, 2020, doi: 10.1109/IFCS-ISAF41089.2020.9234925.